

# A three-dimensional computation of the force and torque on an ellipsoid settling slowly through a viscoelastic fluid

By J. FENG<sup>1</sup>, D. D. JOSEPH<sup>1</sup>, R. GLOWINSKI<sup>2</sup> AND T. W. PAN<sup>2</sup>

<sup>1</sup>Department of Aerospace Engineering and Mechanics, and the Minnesota Supercomputer Center, University of Minnesota, Minneapolis, MN 55455, USA

<sup>2</sup>Department of Mathematics, University of Houston, Houston, TX 77204, USA

(Received 10 November 1993 and in revised form 28 July 1994)

The orientation of an ellipsoid falling in a viscoelastic fluid is studied by methods of perturbation theory. For small fall velocity, the fluid's rheology is described by a second-order fluid model. The solution of the problem can be expressed by a dual expansion in two small parameters: the Reynolds number representing the inertial effect and the Weissenberg number representing the effect of the non-Newtonian stress. Then the original problem is split into three canonical problems: the zeroth-order Stokes problem for a translating ellipsoid and two first-order problems, one for inertia and one for second-order rheology. A Stokes operator is inverted in each of the three cases. The problems are solved numerically on a three-dimensional domain by a finite element method with fictitious domains, and the force and torque on the body are evaluated. The results show that the signs of the perturbation pressure and velocity around the particle for inertia are reversed by viscoelasticity. The torques are also of opposite sign: inertia turns the major axis of the ellipsoid perpendicular to the fall direction; normal stresses turn the major axis parallel to the fall. The competition of these two effects gives rise to an equilibrium tilt angle between 0° and 90° which the settling ellipsoid would eventually assume. The equilibrium tilt angle is a function of the elasticity number, which is the ratio of the Weissenberg number and the Reynolds number. Since this ratio is independent of the fall velocity, the perturbation results do not explain the sudden turning of a long body which occurs when a critical fall velocity is exceeded. This is not surprising because the theory is valid only for slow sedimentation. However, the results do seem to agree qualitatively with 'shape tilting' observed at low fall velocities.

---

## 1. Introduction

In many ways the motions of spherical and long particles in viscoelastic and Newtonian fluids are maximally different. A sphere dropped near a wall in a Newtonian fluid will be pushed away from the wall; in a viscoelastic fluid it will be pulled to the wall. Two spheres launched side by side will be sucked together in a viscoelastic fluid but will repel each other in a Newtonian fluid (Joseph *et al.* 1994). Spheres which are pulled by a small component of gravity onto a plane wall tilted slightly away from the vertical will rotate down the wall normally in a Newtonian liquid as in the case of a dry wall, but will rotate anomalously in the contrary sense in a viscoelastic liquid (Liu *et al.* 1993). A long particle falling in an infinite domain will settle with its broad side perpendicular to the fall in a Newtonian fluid and parallel to the fall in a viscoelastic fluid (Liu & Joseph 1993; Joseph & Liu 1993).

In a general sense, the orientation of a long body settling in a viscoelastic liquid is determined by a competition between inertia and viscoelasticity, and in many cases the viscoelastic effects are felt as normal stresses (Joseph *et al.* 1992). The competition is a complicated affair; ultimately, at high speeds inertia always dominates and the transition to an inertially dominated flow is fairly abrupt and appears to be associated with a critical value of the viscoelastic Mach number. In this interpretation, the broadside-parallel-to-gravity configurations are subcritical and the broadside-on configurations are supercritical in the viscoelastic liquids.

There are a small number of papers which treat orientations of long bodies in sedimentations and particle interactions in shear flows. These have been reviewed by Liu & Joseph (1993) and will not be discussed here. It may be useful to remark that the prior literature did not frame the peculiar observations reported in terms of the competition of inertia and normal stresses.

The focus of the present paper is on the mechanisms which control the orientation of long bodies in sedimentation. We adopt a reference frame fixed on the particle and the undisturbed flow is assumed steady and uniform, impinging upon the particle from a certain incident angle. The torque on the particle suggests the preferred orientation that the particle would assume in sedimentation. We treat the problem as a perturbation of the state of rest for small sedimentation velocity. A second-order fluid model is used, as it is the universal asymptotic form of general constitutive equations for simple fluids at second order. This allows us to express the solution in a dual expansion in two small parameters: the Reynolds number representing the inertial effect and the Weissenberg number representing the normal stress effect. Then the original problem can be broken into three canonical problems: one is the basic Stokes flow and the others modifications to the basic flow by inertial and normal stress effects. Each of the three problems can be solved numerically using a finite element method with fictitious domain, and the force and torque on the particle can be evaluated.

Leal (1975) and Brunn (1977) used the same regular perturbation to study the orientation of a non-spherical body settling without inertia in a second-order fluid. The zeroth-order problem is the Stokes flow, for which Leal (1975) employed an approximate solution for slender bodies. The first-order force and torque on the body are obtained by virtue of the Lorentz reciprocal theorem without actually solving for the velocity and pressure fields at this order. His results show that a slender body would fall with its long axis vertical when the inertia is negligible. Because the analytic calculation is rather involved, it is difficult to extract the physical mechanism responsible for the preferred orientation. In particular, the behaviour of the particle cannot be related to the flow field around it because the first-order solution is not available. The numerical simulation presented in this paper has several advantages over the analytical results in the literature. First, the velocity, pressure and stress distributions at the first order are obtained explicitly; these are important in understanding the mechanisms through which viscoelasticity and inertia alter the fluid flow and in turn affect the motion of the solid body. In addition, both the inertial and the normal stress effects are retained in our computation so that their competition can be assessed. Finally, the numerical solution is not restricted by the aspect ratio of the ellipsoid.

## 2. Formulation of the problem

We consider an axisymmetric ellipsoid of aspect ratio 2:1 fixed in space. Its major and minor axes are  $a$  and  $b = a/2$ . The computational domain is taken to be

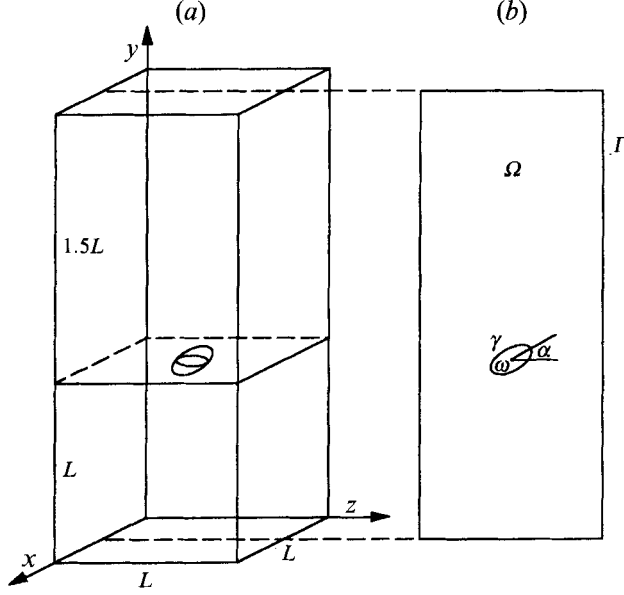


FIGURE 1. (a) The geometry of the three-dimensional boundary value problem.  
 (b) The symmetry plane at  $x = 0.5L$ .

a rectangular box enclosing the ellipsoid (figure 1). The bottom of the box is a square with each side  $L = 4a$ , and its height is  $2.5L$ . The ellipsoid is centred at  $(x_c, y_c, z_c) = (0.5L, L, 0.5L)$ , with its major axis lying in the vertical plane  $x = 0.5L$  and making an angle  $\alpha$  with the horizontal. A uniform flow of velocity  $Ue_y$  is coming from  $y = -\infty$  toward the particle. All six faces of the box are assumed to be undisturbed by the particle and the uniform velocity  $Ue_y$  is imposed as a Dirichlet boundary condition. Obviously, the walls are not far enough from the particle and will increase the drag and torque on the particle. Numerical tests show that larger computational domains become very expensive. So we will settle for the  $L/a = 4:1$  blockage ratio. If the effect of blockage is equivalent to an increased fluid velocity, then the preferred orientation of the ellipsoid will not be affected, as will be evidenced by equations (8) and (16).

The velocity  $u$  and pressure  $p$  of the flow field around the body is determined by the following boundary value problem:

$$\left. \begin{aligned} \nabla \cdot u &= 0, & \rho u \cdot \nabla u &= \nabla \cdot T, \\ T &= -\rho I + \mu \mathbf{A}_1 + \alpha_1 \mathbf{A}_2 + \alpha_2 \mathbf{A}_1^2, \\ u|_r &= Ue_y, & u|_\gamma &= 0, \end{aligned} \right\} \quad (1)$$

where  $\rho$ ,  $\mu$ ,  $\alpha_1$  and  $\alpha_2$  are the density, shear viscosity, the first and second quadratic constants of the second-order fluid;  $\Gamma$  is the outer boundary and  $\gamma$  is the surface of the body.  $\mathbf{A}_1$  and  $\mathbf{A}_2$  are the first- and second-order Rivlin-Ericksen tensors. We define dimensionless variables (indicated by an asterisk) by

$$u = u^*U, \quad \nabla = \frac{\nabla^*}{a}, \quad \mathbf{A}_1 = \mathbf{A}_1^* \frac{U}{a}, \quad \mathbf{A}_2 = \mathbf{A}_2^* \frac{U^2}{a^2}, \quad p = p^* \frac{\mu U}{a}.$$

Then problem (1) can be re-written as (the asterisk omitted hereafter)

$$\left. \begin{aligned} \nabla \cdot u &= 0, \\ \nabla p - \nabla^2 u &= -R(u \cdot \nabla u) - W \nabla \cdot (\mathbf{A}_2 + \epsilon \mathbf{A}_1^2), \\ u|_r &= e_y, & u|_\gamma &= 0, \end{aligned} \right\} \quad (2)$$

where  $R = \rho Ua/\mu$  is the Reynolds number,  $W = -\alpha_1 U/\mu a$  is the Weissenberg number and  $\epsilon = \alpha_2/\alpha_1$ . For most polymer solutions,  $\alpha_1 < 0$ ,  $\alpha_2 > 0$ , so that  $W > 0$  and  $\epsilon < 0$ . We use a typical value  $\epsilon = -1.87$  suggested by Joseph (1990, p. 516) for the case in which the second normal stress coefficient is  $-1/15.4$  of the first. The Weissenberg number can be considered as the limiting zero-shear value of the ratio of normal stress to shear stress. This ratio may be related to the rod-climbing constant  $\tilde{\beta}$ , which is readily measurable in experiments (Joseph 1990):

$$W = \frac{N_1}{\tau} = \frac{-\alpha_1(U/a)^2}{\mu(U/a)} = -\frac{\alpha_1 U}{\mu a} = \frac{1.35\tilde{\beta} U}{\mu a}.$$

Assuming  $R \ll 1$ ,  $W \ll 1$ , the solution to (2) can be expressed as

$$\left. \begin{aligned} \mathbf{u} &= \mathbf{u}_0 + R\mathbf{u}_1 + W\mathbf{u}_2 + \text{second- and higher-order terms,} \\ p &= p_0 + Rp_1 + Wp_2 + \text{second- and higher-order terms.} \end{aligned} \right\} \quad (3)$$

Then problem (2) can be broken into three problems if we keep the first-order terms in  $R$  and  $W$  only:

$$\left. \begin{aligned} \text{Stokes problem: } \quad \nabla \cdot \mathbf{u}_0 &= 0, & \nabla p_0 - \nabla^2 \mathbf{u}_0 &= \mathbf{0}, \\ \mathbf{u}_0|_{\Gamma} &= \mathbf{e}_y, & \mathbf{u}_0|_{\gamma} &= \mathbf{0}; \end{aligned} \right\} \quad (4)$$

$$\left. \begin{aligned} \text{Inertial perturbation: } \quad \nabla \cdot \mathbf{u}_1 &= 0, \\ \nabla p_1 - \nabla^2 \mathbf{u}_1 &= -(\mathbf{u}_0 \cdot \nabla \mathbf{u}_0), \\ \mathbf{u}_1|_{\Gamma+\gamma} &= \mathbf{0}; \end{aligned} \right\} \quad (5)$$

$$\left. \begin{aligned} \text{Normal stress perturbation: } \quad \nabla \cdot \mathbf{u}_2 &= 0, \\ \nabla p_2 - \nabla^2 \mathbf{u}_2 &= -\nabla \cdot (\mathbf{A}_2 + \epsilon \mathbf{A}_1^2)|_{\mathbf{u}_0}, \\ \mathbf{u}_2|_{\Gamma+\gamma} &= \mathbf{0}. \end{aligned} \right\} \quad (6)$$

The stress tensor can be written as

$$\begin{aligned} \mathbf{T} &= [-p_0 \mathbf{I} + \mathbf{A}_1(\mathbf{u}_0)] + R[-p_1 \mathbf{I} + \mathbf{A}_1(\mathbf{u}_1)] + W[-p_2 \mathbf{I} + \mathbf{A}_1(\mathbf{u}_2) - (\mathbf{A}_2 + \epsilon \mathbf{A}_1^2)|_{\mathbf{u}_0}] \\ &= \mathbf{T}_0 + R\mathbf{T}_1 + W\mathbf{T}_2, \end{aligned} \quad (7)$$

and the dimensionless force and torque on the body are

$$\left. \begin{aligned} \mathbf{F} &= \int_{\gamma} \mathbf{n} \cdot \mathbf{T} \, dA = \mathbf{F}_0 + R\mathbf{F}_1 + W\mathbf{F}_2, \\ \mathbf{M} &= \int_{\gamma} (\mathbf{r} - \mathbf{r}_c) \times (\mathbf{n} \cdot \mathbf{T}) \, dA = \mathbf{M}_0 + R\mathbf{M}_1 + W\mathbf{M}_2. \end{aligned} \right\} \quad (8)$$

Note that the dimensional force is proportional to the dimensionless force multiplied by  $U$ . There is an additional  $U$ -factor in  $R$  and  $W$  so that the dimensional drags due to inertia and viscoelasticity are proportional to  $U^2$ . Since the total drag must change sign when  $U$  does,  $\mathbf{F}_1$  and  $\mathbf{F}_2$  are necessarily zero for particles with fore-aft symmetry. A similar argument leads to  $\mathbf{M}_0 = \mathbf{0}$ , a well-known result for Stokes flow. Leslie (1961) showed that the first-order contribution of viscoelasticity to the drag on a sphere vanishes. The same result for slender bodies with fore-aft symmetry was obtained by Leal (1975).

### 3. Numerical method

The fictitious domain method has been used to solve boundary value problems on multiply-connected domains. The basic idea is to convert the original problem into a new one posed on an auxiliary domain of a simple shape which contains the actual

domain. Then structured mesh and fast solvers can be used on the auxiliary domain. The application of this method to incompressible viscous flows has been explored by Glowinski, Pan & Periaux (1994). In our case, we need to solve the three Stokes type of problems (4), (5) and (6). The basic procedure is explained as follows.

Consider a Stokes type of boundary value problem posed on a domain shown in figure 1:

$$\left. \begin{aligned} \nabla \cdot \mathbf{u} = 0, \quad \nabla p - \nabla^2 \mathbf{u} = \mathbf{f} \quad \text{in } \Omega \setminus \omega, \\ \mathbf{u}|_\gamma = \mathbf{g}_2 \quad \left( \text{with } \int_\Gamma \mathbf{g}_1 \cdot \mathbf{n} \, dA + \int_\gamma \mathbf{g}_2 \cdot \mathbf{n} \, dA = 0 \right), \end{aligned} \right\} \quad (9)$$

where  $\Omega$  is the entire domain enclosed by the rectangular box  $\Gamma$  and  $\omega$  is the sub-domain inside the ellipsoid. The surface of the ellipsoid is  $\gamma$ ;  $\mathbf{f}$  represents the perturbation terms in (5) and (6). For a clearer view, we have put these symbols in a two-dimensional domain (figure 1b). The procedure outlined below applied, of course, to both two- and three-dimensional problems.

We embed the multiply-connected domain  $\Omega \setminus \omega$  in  $\Omega$ . If  $\tilde{\mathbf{f}}$  is an extension of  $\mathbf{f}$  in  $\Omega$ , then (9) is equivalent to the following problem on the entire domain  $\Omega$ :

$$\begin{aligned} \text{Find } U \in (H^1(\Omega))^3, P \in \{q \mid q \in L^2(\Omega), \int_\Omega q \, dV = 0\}, \lambda \in (L^2(\gamma))^3, \text{ such that} \\ \int_\Omega \nabla U \cdot \nabla v \, dV - \int_\Omega P \nabla \cdot v \, dV = \int_\Omega \tilde{\mathbf{f}} \cdot v \, dV + \int_\gamma \lambda \cdot v \, dA, \quad \forall v \in (H_0^1(\Omega))^3, \\ \nabla \cdot U = 0, \\ U|_\Gamma = \mathbf{g}_1, \quad U|_\gamma = \mathbf{g}_2. \end{aligned}$$

The solution to (9) is, then,  $\mathbf{u} = U|_{\Omega \setminus \omega}$ ,  $p = P|_{\Omega \setminus \omega}$ . Note that the effect of the actual geometry is contained in  $\int_\gamma \lambda \cdot v \, dA$  and in the second boundary condition.

The above problem on the fictitious domain is solved using a conjugate gradient algorithm, which is explained in detail by Glowinski *et al.* (1994). Because of the simple geometry, a regular mesh is used. The rectangular box is cut into cubes of side  $h = L/I_h$ , and each cube is cut into 6 tetrahedrons, which are the finite elements in the solution of the elliptic problems arising from the conjugate gradient algorithm. The accuracy is believed to be of second order in  $h/L$ . To compute the surface integral  $\int_\gamma \lambda \cdot v \, dA$ , the surface of the ellipsoid is cut into  $N$  pieces by uniformly dividing the two angular coordinates  $\theta$  and  $\phi$  (figure 2), such that the length of the sides for each piece is roughly equal to the linear dimension of the elements  $h$ . The multiplier vector  $\lambda$  is taken to be constant on each piece. The right-hand-side terms in (5) and (6) are evaluated using second-order finite difference schemes.

Because of the regular structure of the mesh, the surface of the particle is usually not represented by grid points, and the force and torque cannot be directly computed by the surface integrals in (8). We use the Gauss theorem to convert the surface integral on the ellipsoid into the summation of a surface integral on the enclosing box  $\Gamma$  and a volume integral on the volume occupied by the fluid:

$$\mathbf{F} = - \int_\Gamma \mathbf{n} \cdot \mathbf{T} \, dA - \int_{\Omega \setminus \omega} \nabla \cdot \mathbf{T} \, dV, \quad (10)$$

where  $\mathbf{n}$  is the inner normal vector on the six faces of the box. The volume integration

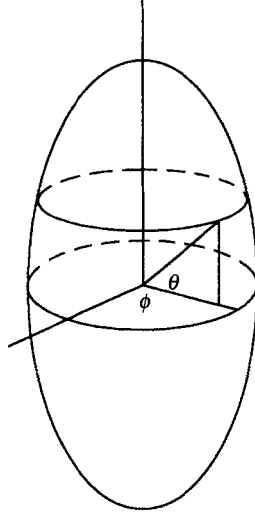


FIGURE 2. The surface of the ellipsoid is cut into square-like pieces using the two angles  $\phi$  and  $\theta$ .

is done by adding up the contribution from the eight vertices in each cube. If any vertex is inside the ellipsoid, its contribution is excluded. To calculate the torque, we write

$$(\mathbf{r} - \mathbf{r}_c) \times (\mathbf{n} \cdot \mathbf{T}) = \mathbf{n} \cdot \boldsymbol{\tau},$$

where the tensor  $\boldsymbol{\tau}$  is defined by

$$\tau_{jk} = -x_i T_{jl} \epsilon_{ilk},$$

$x_i$  being the components of  $\mathbf{r} - \mathbf{r}_c$ . Note that we use a left-hand coordinate system that gives the minus sign to the permutation tensor. Then the torque on the particle can be computed by

$$\mathbf{M} = - \int_{\Gamma} \mathbf{n} \cdot \boldsymbol{\tau} \, dA - \int_{\Omega \setminus \omega} \nabla \cdot \boldsymbol{\tau} \, dV. \quad (11)$$

Because of the error associated with the high-order differentiation in  $\nabla \cdot \mathbf{T}$ , the Stokes drag on the ellipsoid can be more accurately computed by studying the momentum balance in the fluid flow. As uniform flow is assigned to the inlet ( $y = 0$ ) and outlet ( $y = 2.5L$ ) of the domain, the net momentum flux vanishes and the drag can be found from the pressure difference between the inlet and the outlet and the shear stress (denoted by  $t$ ) on the four side walls:

$$F_y = \int_{inlet} p \, dA - \int_{outlet} p \, dA - \int_{sides} t \, dA.$$

The torque  $\mathbf{M}$  has to be computed directly from (11).

A typical mesh ( $I_n = 50$ ) has 330 327 grid points,  $1.89 \times 10^6$  tetrahedron elements and about 40 pieces on the particle. Each of the three problems takes about 60 minutes on a Cray-XMP supercomputer.

## 4. Numerical results and discussion

### 4.1. Drag on a sphere

To test the accuracy of the scheme for calculating  $\mathbf{F}$ , we first compute the Stokes flow around a sphere as a test case. The sphere is located at  $(x_c, y_c, z_c) = (0.5, 1, 0.5) L$ , and its diameter is  $d = 0.25L$ . The sidewalls increase the drag on the sphere because of

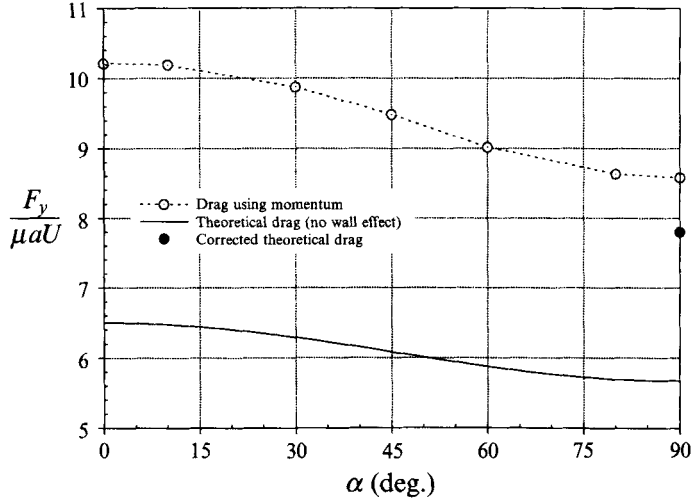


FIGURE 3. Drag on the ellipsoid at different tilt angles. The theoretical result without wall effect (Happel & Brenner 1986, p. 223):  $F_y = \mu a U (5.672 + 0.828 \cos^2 \alpha)$  is also shown for comparison.

blockage of the flow area. To use the theoretical result for a sphere at the centre of a circular cylinder, we have to convert the area blockage ratio to an effective radius ratio. If we use an effective radius that gives the same area  $L^2$ , a corrected Stokes drag coefficient is obtained for the parameters used here (Happel & Brenner 1986, p. 318):

$$C_d = 43.178/R.$$

The result of our calculation is about 6.9% higher than the corrected Stokes drag. If we use the radius of the inscribed circle, the corrected Stokes drag coefficient is only 2% higher than our computation, suggesting that this radius represents the actual blockage better. We have also tested a smaller sphere ( $d = 0.125L$ ), and the drag is again between the Stokes drags corrected using the inscribed circle and the equi-area circle. No better comparison is available, and the numerical tests give us a rough idea of the accuracy of the force calculation.

#### 4.2. Drag and torque on the ellipsoid

The ellipsoid is fixed at seven different tilt angles:  $\alpha = 0^\circ, 10^\circ, 30^\circ, 45^\circ, 60^\circ, 80^\circ$  and  $90^\circ$ , and the Stokes, inertial perturbation and normal stress perturbation problems are solved. First, let us look at the forces on the body. The drag and lift obtained in the Stokes problem are compared to the theoretical results of Happel & Brenner (1986) in figures 3 and 4. The estimation of the wall effect on the drag is only possible when the ellipsoid lies axisymmetrically on the centre of a circular cylinder and its major axis is much smaller than the diameter of the cylinder (Happel & Brenner 1986, p. 338). This corresponds to  $\alpha = 90^\circ$  in our problem, but the ratio of length here is not sufficiently small ( $= 0.22$  for the radius of the equi-area circle). Based on this ratio, the asymptotic formula gives a correction factor of 1.376 for the drag, which underestimates the wall effect. Our computation yields a value about 9% higher than the corrected drag (figure 3). At smaller tilt angles, the wall effect should be larger, but no relevant theoretical results are available for comparison. The Stokes lift from our computation, however, agrees relatively well with the theoretical result (figure 4). The inertia and normal stress perturbations give a drag on the order of  $10^{-8}$  and  $10^{-4}$ , respectively. Because these should be identically zero, their values represent the typical error in our calculations.

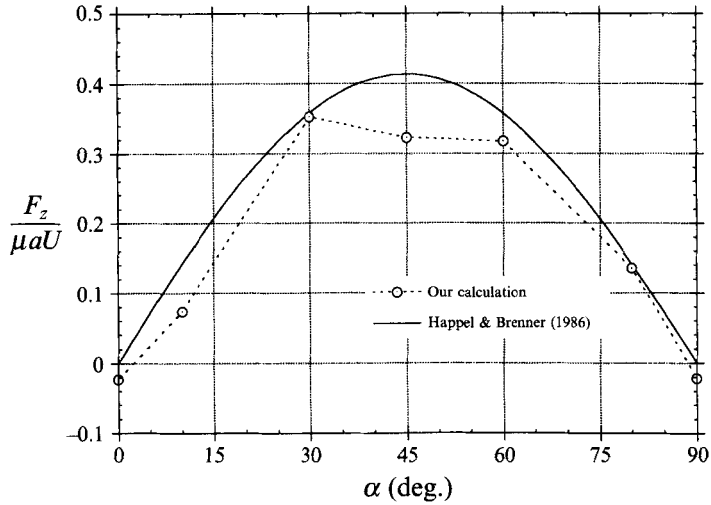


FIGURE 4. Life on the ellipsoid at different tilt angles. The theoretical result (Happel & Brenner 1986):  $F_z = 0.828\mu aU \sin \alpha \cos \alpha$  is also shown for comparison.

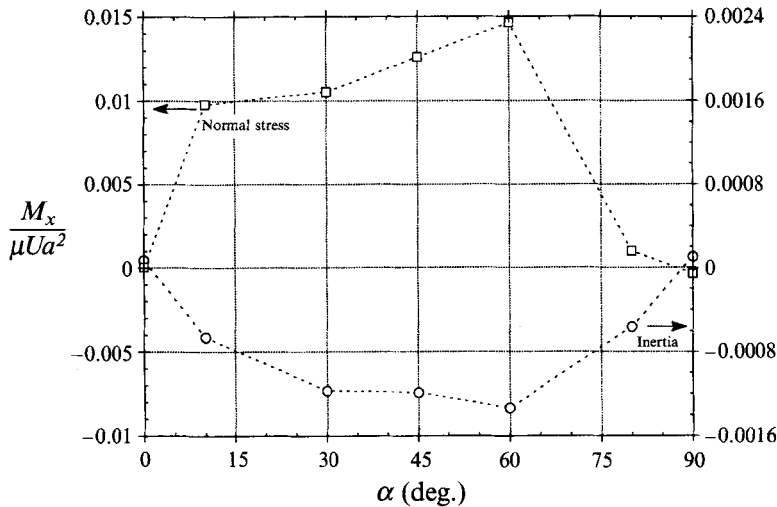


FIGURE 5. The torques on the ellipsoid caused by the inertial perturbation and the normal stress perturbation.

We now turn our attention to the torque on the ellipsoid. For the Stokes flow, the torque should vanish identically. Our calculation gives torque components on the order of  $10^{-6}$ . For the inertial and normal stress perturbations, the  $y$ - and  $z$ -components of the torque should also vanish because of symmetry. Their values in our computation are typically on the order of  $10^{-5}$ . This is regarded as the typical error in our torque calculations. Figure 5 shows the  $x$ -component of the torque for different tilt angles obtained from the inertial and normal stress perturbations.

At any tilt angle  $0^\circ < \alpha < 90^\circ$ , inertia exerts a negative torque on the ellipsoid which turns it broadside-on. This effect is well known both from perturbation with weak inertia (Cox 1965) and from direct numerical simulations at moderately large Reynolds

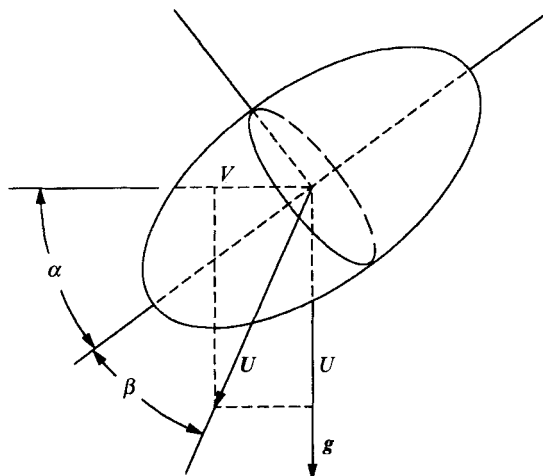


FIGURE 6. The sideways drift of an ellipsoid.  $\alpha$  is the tilt angle and  $\beta$  is the angle between the symmetry axis of the particle and the direction of its falling velocity.

numbers (Feng, Hu & Joseph 1994). The normal stress applies a positive torque which turns the ellipsoid to a vertical head-on configuration. This effect has been obtained by the perturbation theories of Leal (1975). The torque due to normal stress is typically one order of magnitude larger than that due to inertia.

Since Cox's (1965) result is for a spheroid of small eccentricity (near-sphere) and Leal's (1975) is for a slender body, direct comparison with figure 5 is not appropriate. However, we notice that the torque has the same form in both limiting cases:

$$\left. \begin{aligned} \text{Cox: } M_x &= -K_1 R \sin \beta \cos \beta, \\ \text{Leal: } M_x &= K_2 W \sin \beta \cos \beta, \end{aligned} \right\} \quad (12)$$

where  $K_1$  and  $K_2$  are positive constants;  $\beta$  is the angle between the symmetry axis of the body and the direction of free sedimentation, which is related to our tilt angle  $\alpha$  by  $\tan \alpha \tan \beta = K_3 < 1$ ,  $K_3$  depending on the shape of the body (see Leal 1975, pp. 309, 335). If one assumes that the form in (12) holds for a more general ellipsoid, then for both inertial and normal stress perturbations

$$M_x \propto \frac{\sin \alpha \cos \alpha}{\sin^2 \alpha + K_3^2 \cos^2 \alpha},$$

which gives a larger torque for angles  $\alpha < 45^\circ$  than  $90^\circ - \alpha$ . This is true in figure 5 except for the point  $\alpha = 60^\circ$ . We refined the mesh to check this. The magnitudes of  $M_y$ ,  $M_z$  and  $M_0$  are further reduced for the finer mesh, but  $M_x$  does not change appreciably. Our conjecture is that the asymptotic results (12) cannot be generalized to ellipsoids of intermediate aspect ratio.

#### 4.3. Equilibrium tilt angle

We now consider how the torques in figure 5 can be related to the orientation of the ellipsoid when it settles steadily in an infinite expanse of fluid. In Stokes flow, the ellipsoid will migrate laterally while settling (figure 6):

$$V/U = \tan(\alpha + \beta). \quad (13)$$

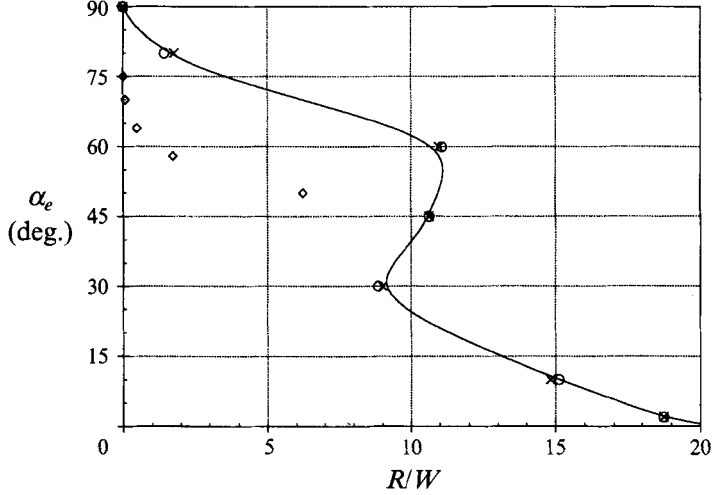


FIGURE 7. The equilibrium tilt angle as a function of the ratio of the Reynolds number to the Weissenberg number. This ratio is related to the climbing constant by  $R/W = 0.741\rho a^2/\beta$ .  $\circ$ , Data points computed from (15) and the solid line is a smoothed curve-fitting to the circles;  $\times$ , data points obtained by neglecting the sidewise drift of the particle;  $\diamond$ , experimental points from Liu & Joseph (1993) (the last point at  $R/W = 6.25$  corresponds to  $R = 3.6$ , which is out of the range of the perturbation theory).

As  $\tan \alpha \tan \beta = K_3$ ,  $V$  can be expressed by the shape and the orientation of the particle:

$$V = \frac{U(1-K_3)}{\tan \alpha + K_3/\tan \alpha}. \quad (14)$$

Now the torque on the ellipsoid can be computed as the sum of two components of the flow:

$$M_x = R_U M_x^{(1)}(\alpha) + W_U M_x^{(2)}(\alpha) - R_V M_x^{(1)}(\frac{1}{2}\pi - \alpha) - W_V M_x^{(2)}(\frac{1}{2}\pi - \alpha),$$

where  $R_U, W_U$  are the Reynolds number and Weissenberg number computed using  $U$ , and  $R_V, W_V$  are those using  $V$ . Eliminating  $R_V, W_V$  using (14) and writing  $R_U, W_U$  as  $R$  and  $W$ , we have

$$M_x(\alpha) = R \left\{ M_x^{(1)}(\alpha) - \frac{1-K_3}{\tan \alpha + K_3/\tan \alpha} M_x^{(1)}(\frac{1}{2}\pi - \alpha) \right\} + W \left\{ M_x^{(2)}(\alpha) - \frac{1-K_3}{\tan \alpha + K_3/\tan \alpha} M_x^{(2)}(\frac{1}{2}\pi - \alpha) \right\}. \quad (15)$$

An equilibrium tilt angle  $\alpha_e$  can be defined by

$$M_x(\alpha_e) = 0. \quad (16)$$

The geometric parameter  $K_3$  can be computed from the drag forces on the ellipsoid when its symmetry axis is parallel and perpendicular to a uniform stream (Happel & Brenner 1986, p. 223). For aspect ratio = 2:1, we get  $K_3 = 0.8731$ . This gives us the smoothed curve in figure 7. Data points computed by neglecting the lateral drift are also shown. The effect of sidewise drift on the equilibrium orientation is minimal. This is because the aspect ratio of the ellipsoid is not large and there is a certain degree of symmetry about  $45^\circ$  in the two curves of figure 5.

The competition between inertia and normal stresses is represented by the elasticity number of the fluid  $E = W/R$  and is independent of the particle's velocity. This is consistent with the fact that the present result is valid only for slow sedimentation. The competition can also be demonstrated by a ratio of lengths: a length typical of gradient, such as the characteristic length of the body  $a$ , and a material length expressed by, say,  $(-\alpha_1/\rho)^{1/2}$  (see Joseph 1990, §17.1, p. 483). We can assert that the length  $l = (\beta/\rho)^{1/2}$  is a suitable measure of the material length. When  $a/l$  is small, normal stresses dominate; when  $a/l$  is large, inertia dominates.

Curiously, the curve in figure 7 predicts multiple equilibrium orientations for a small range of  $R/W$ . Let us consider the stability of these tilt angles. The effect of sidewise drift will be neglected and the equilibrium tilt angle satisfies

$$M_x(\alpha_e) \approx RM_x^{(1)}(\alpha_e) + WM_x^{(2)}(\alpha_e) = 0. \quad (17)$$

Because of the definitions of the angle  $\alpha$  and the sign of the torque, an equilibrium  $\alpha_e$  is stable if

$$\left. \frac{dM_x}{d\alpha} \right|_{\alpha_e} = R \left. \frac{dM_x^{(1)}}{d\alpha} \right|_{\alpha_e} + W \left. \frac{dM_x^{(2)}}{d\alpha} \right|_{\alpha_e} + \left( M_x^{(1)} \frac{dR}{d\alpha} + M_x^{(2)} \frac{dW}{d\alpha} \right) \Big|_{\alpha_e} < 0.$$

The dependence of  $R$  and  $W$  on  $\alpha$  arises because the fall velocity  $U$  depends on the orientation of the ellipsoid in free settling. Since  $R$  and  $W$  are linear in  $U$ , the two terms in the parentheses cancel out owing to (17). Then, we can write

$$\left. \frac{dM_x}{d\alpha} \right|_{\alpha_e} = RM_x^{(2)} \left. \frac{d}{d\alpha} \left( \frac{M_x^{(1)}}{M_x^{(2)}} \right) \right|_{\alpha_e}.$$

Noting that figure 7 is actually a plot of  $-M_x^{(2)}(\alpha)/M_x^{(1)}(\alpha)$  versus  $\alpha$ , we observe that within an interval of  $\alpha$  around  $45^\circ$ ,

$$\frac{d}{d\alpha} \left( \frac{M_x^{(1)}}{M_x^{(2)}} \right) > 0.$$

This interval can be tentatively set to be from  $30^\circ$  to  $60^\circ$ . The exact range is unknown at this point since we have tested only five different angles between  $0^\circ$  and  $90^\circ$ . Because  $R > 0$ ,  $M_x^{(2)} > 0$ , the equilibrium tilt angles within this range are unstable, giving rise to a hysteresis loop. This surprising result has not yet been tested by experiments. In fact, for the ratio  $R/W$  to get into the range of the kink in figure 7 ( $R/W \approx 10$ ), the climbing constant  $\beta$  has to be very small. For instance, if  $\rho = 1 \text{ g cm}^{-3}$  and  $a = 1 \text{ cm}$ ,  $\beta$  must be as small as  $0.07 \text{ g cm}^{-1}$ . The smallest climbing constant measured by Joseph *et al.* (1994) is about  $0.97 \text{ g cm}^{-1}$  for STP. Thus, the experimental verification of this phenomenon will be a delicate and difficult matter. We also note that the range of unstable tilt angles may depend on the shape of the particle if the effect of sidewise drift is considered.

If one uses the analytical results of Cox (1965) and Leal (1975) to define an equilibrium tilt angle (equation (12)), then  $\alpha_e$  would be zero for elasticity numbers below a critical value, and would jump to  $90^\circ$  when this critical value is exceeded. Experiments on very slow sedimentations have shown, however, that intermediate tilt angles do exist and they are very sensitive to the shape of the particle (Liu & Joseph 1993). This again suggests that the asymptotic forms of (12) may not apply to an ellipsoid of a moderate aspect ratio. Finally it should be pointed out that the results given here are subject to wall effects due to the finite volume of our computational

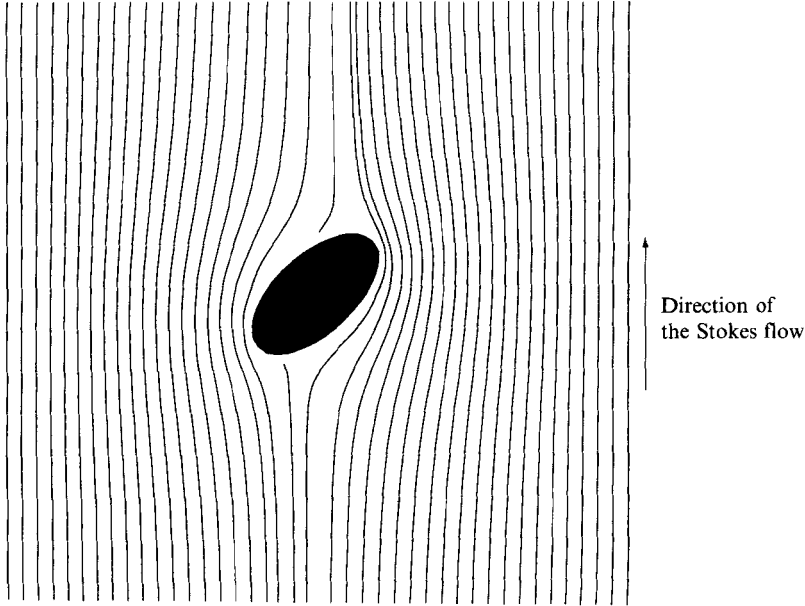


FIGURE 8. Streamlines on the symmetry plane for the Stokes flow around the ellipsoid posed at  $\alpha = 45^\circ$ . Two 'stagnation points' with pressure extrema can be found at the front and the back of the body.

domain. If the wall effects amount to an increased fall velocity, the data in figure 7 will still be valid for an infinite domain. In addition, since the particle is in the centre of the domain, we expect the walls not to affect the turning of the ellipsoid very much.

#### 4.4. Analysis of the flow fields

We can gain further knowledge of the opposing effects of inertia and normal stress by studying the flow fields around the particle. Figure 8 shows streamlines of the Stokes flow on the symmetry plane ( $x = 0.5$ ) for  $\alpha = 45^\circ$ . Two stagnation points can be identified on the front and the back of the body where pressure  $p_0$  has a maximum and a minimum. The stagnation points are also distinguished points for the perturbation velocities shown in figures 9(a) and 9(b) and for the perturbation pressure in figures 10(a) and 10(b). The perturbation velocity for inertia,  $\mathbf{u}$ , is such that the fluid impinges upon the particle at the two points of stagnation. The perturbation pressure for inertia,  $p_1$ , is maximum at these two points; its distribution explains the negative torque created by inertia. The direction of the velocity  $\mathbf{u}_2$ , associated with viscoelastic perturbation, is opposite to  $\mathbf{u}_1$ ; two streams come toward the body from the left and the right and the fluid flows away from the stagnation points along the stagnation streamlines of the Stokes flow. The perturbation pressure for viscoelasticity is opposite to  $p_1$ ; it gives rise to a suction at the stagnation points which has the effect of turning the long side of the ellipsoid parallel to the stream, consistent with observations. For Stokes flow, the velocity and pressure have different signs at the front and rear stagnation points. The inertial and viscoelastic perturbations, however, produce velocity and pressure that have the same sign at the front and the rear. This is consistent with the parity of linear and quadratic perturbations of rest.

The results exhibited in figures 9 and 10 show that the differences between Newtonian and viscoelastic fluids are maximal in the sense that every flow quantity which we computed changes its sign. Not only the overall torques, but the pressure and

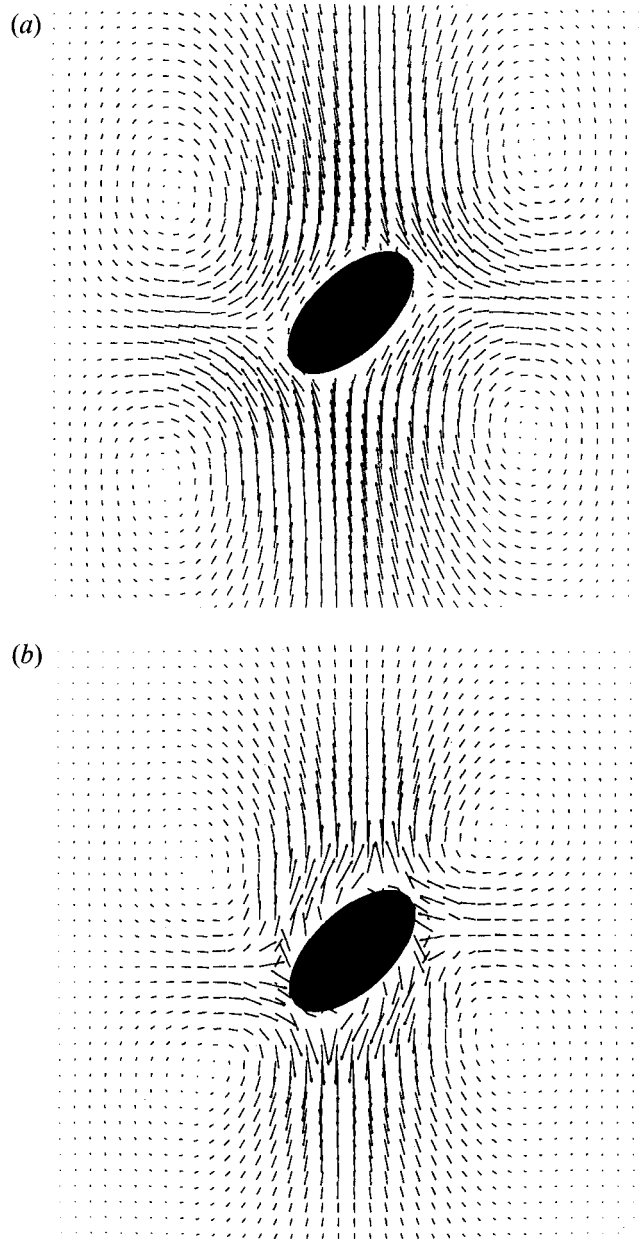


FIGURE 9. (a) Velocity field on the symmetry plane due to inertial perturbation.  $\alpha = 45^\circ$ . (b) Velocity field on the symmetry plane due to normal stress perturbation.  $\alpha = 45^\circ$ . The magnitude of  $u_2$  is much larger than that of  $u_1$ , and the velocity is scaled differently in (a) and (b).

velocity components at nearly all points on the body have different signs in Newtonian and viscoelastic flows. We are compelled to believe that the contrary behaviours of particles settling in Newtonian and viscoelastic fluids are associated with the ubiquitous changing of sign.

The above analysis centres around the pressure distribution and does not include the effects of shear and extra normal stresses. For the inertial perturbation, the viscous normal stress vanishes on the solid surface. It is natural that the inertia of the fluid is

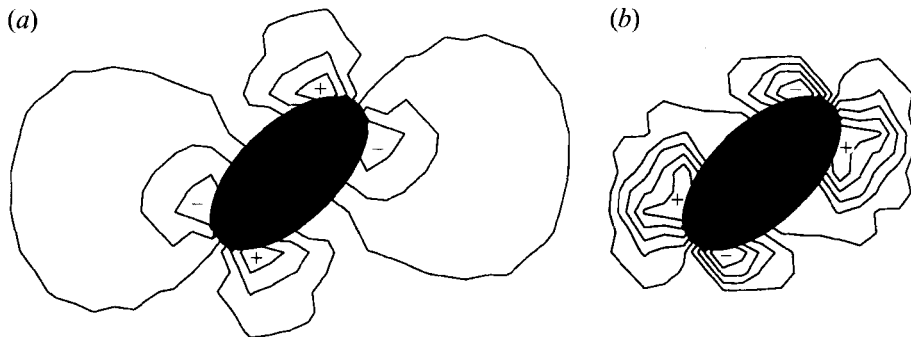


FIGURE 10. (a) Pressure contours on the symmetry plane due to inertial perturbation. The velocity field  $\mathbf{u}_1$  causes two high pressures (marked by ‘plus’ signs) and two low pressures (marked by ‘minus’ signs) on the surface of the ellipsoid which give rise to a negative torque. (b) Pressure contours on the symmetry plane due to normal stress perturbation. The velocity field  $\mathbf{u}_2$  causes two high pressures (marked by ‘plus’ signs) and two low pressures (marked by ‘minus’ signs) on the surface of the ellipsoid which give rise to a positive torque.

manifested by the pressure (figure 10a), which then produces the negative torque. One would think that the major effect of viscoelasticity in turning a long body should come from the normal stress term  $\mathbf{A}_2 + \epsilon \mathbf{A}_1^2|_{\mathbf{u}_0}$ . But this turns out not to be the case. We have evaluated the effect of each term multiplying  $W$  in (7) which arises from the perturbation of the Stokes flow by viscoelasticity (6). The dominant contribution to the positive torque is from the pressure  $p_2$ . the term  $\mathbf{A}_1(\mathbf{u}_2)$  is basically neutral and  $\mathbf{A}_2 + \epsilon \mathbf{A}_1^2|_{\mathbf{u}_0}$  leads to weak broadside-on turning, opposing  $p_2$ . Therefore, analysing the distributions of  $p_1$  and  $p_2$  is sufficient in explaining the opposing torques exerted by inertia and viscoelasticity.

It is perhaps relevant to mention an earlier attempt at interpreting the turning of a long body by viscoelasticity. Joseph (1992) and Joseph *et al.* (1992) used a potential flow field to evaluate the normal stress at a stagnation point. They showed that the second-order term gives a positive (tensile) contribution to the normal stress and surmized that this may be the mechanism that turns the long side of the particle parallel to the stream. This argument does not apply to our problem because the normal stress from the second-order term vanishes at the stagnation point because of the no-slip condition, which a potential flow does not satisfy.

## 5. Discussion of experiments

Liu & Joseph (1993) and Joseph & Liu (1993) did experiments on the settling of long bodies. They documented a tilt transition which is associated with a critical value of the fall velocity  $U$  in a viscoelastic fluid. The phenomenon appears to correlate with the viscoelastic Mach number, with the particle’s nose down when the settling velocity is less than the shear wave speed of the liquid measured on the wave speed meter ( $M < 1$ ), and broadside on for larger  $U$ . The transition is rather abrupt, and the plots of the experimental data resemble a structured shock wave with data on the curve representing a smooth connection between the two distinct states.

Obviously, the tilt transition is a process different from the prediction given here based on the competition between weak normal stress and weak inertia that perturb a Stokes flow. In the limit of slow motion ( $R \ll 1$  and  $W \ll 1$ ), the equilibrium orientation is determined by the elasticity number and is independent of the settling velocity. The dynamic tilt transition, on the other hand, is dictated by the Mach

number and concerns the propagation of a discontinuity in a viscoelastic medium. It is well known that such dynamic properties may not be preserved when the constitutive equation degenerates into an asymptotic form, such as the second-order fluid model, under extreme conditions (Astarita & Marrucci 1975, p. 276). Therefore, the apparent disagreement between the present result and experiments at high Reynolds and Weissenberg numbers is understandable.

In a set of sedimentation tests at extremely low speeds, Liu & Joseph (1993) did observe an equilibrium tilt angle between  $0^\circ$  and  $90^\circ$ . These tilt angles are not strongly dependent on velocity until the Mach number passes through unity, when they change dramatically. They are also very sensitive to the shape of the particle and so were named 'shape tilting'. Figure 7 shows a few points from Liu & Joseph (1993) for an aluminium cylinder with flat ends settling in aqueous polyox. Shape tilting may be related to a kind of competition between inertia and normal stresses which arises in perturbation analysis and for which the elasticity number is the important parameter.

In summary, there are two kinds of competition. The first is that predicted by the present study which prevails when  $R \rightarrow 0$  and  $W \rightarrow 0$ . In this case, the competition is resolved by an elasticity number  $E = W/R$ . The other kind of competition is represented by the tilt transition observed in experiment when  $M = (RW)^{1/2} > 1$ , which may be related to change of type when the fall velocity exceeds the speeds at which signals can propagate into rest. This type of competition is dynamic, and occurs for critical values of  $U$  in a family of fluids with different elasticity numbers.

In closing, it should be pointed out that nose-down settling has also been reported in viscoelastic liquids without measurable normal stress differences, for example, in 0.39% aqueous Xanthan and in 0.4% Carbopol in 50% aqueous glycerin (Joseph & Liu 1993). These experiments suggest that the memory of shear thinning leads to corridors of reduced viscosity through which a long particle settles more easily with its long side parallel to the fall. This is yet another mechanism potentially responsible for turning a long body in a viscoelastic fluid.

## 6. Conclusions

We have computed the force and torque on an ellipsoid settling slowly in a viscoelastic liquid. Although the problem is in steady state, the preferred orientation can be inferred from the torque values. Based on the results presented in this paper, the following conclusions can be drawn.

(i) The turning of a long particle is determined mainly by the pressure at the points of stagnation of the Stokes flow.

(ii) The perturbation pressure and velocity distributions are reversed around the particle for inertia and viscoelasticity.

(iii) This reversal gives rise to turning couples in opposite directions: fluid inertia produces a torque that turns the broadside of the ellipsoid perpendicular to the direction of fall; normal stress gives rise to a torque that turns the broadside of the ellipsoid parallel to the direction of fall.

(iv) Under the mutual actions of inertia and normal stress, the ellipsoid assumes an equilibrium tilt angle between  $0^\circ$  and  $90^\circ$ . Under the assumption of a second-order fluid model, the equilibrium orientation is a function of the ratio of the Reynolds number to the Weissenberg number.

(v) Our numerical results suggest the existence of a range of unstable tilt angles around  $45^\circ$ . This proposition needs to be examined by more detailed computations and experiments.

(vi) If the fall velocity is not vanishingly small, the competition of normal stress and inertia is manifested by the tilt transition, which appears to be related to the mechanism of change of type. This mechanism is not related to the competition predicted by perturbing the Stokes flow.

This work was supported by the NSF, Fluid, Particulate and Hydraulic Systems, by the US Army, Mathematics and AHPCRC, by the DOE, Department of Basic Energy Sciences and the Minnesota Supercomputer Institute. The authors thank Timothy Hall for helping generate the graphics, Adam Huang for stimulating discussions and the referees for valuable criticism and suggestions.

#### REFERENCES

- ASTARITA, G. & MARRUCCI, G. 1974 *Principles of Non-Newtonian Fluid Mechanics*. McGraw-Hill.
- BRUNN, P. 1977 The slow motion of a rigid particle in a second-order fluid. *J. Fluid Mech.* **82**, 529–550.
- COX, R. G. 1965 The steady motion of a particle of arbitrary shape at small Reynolds numbers. *J. Fluid Mech.* **23**, 625–643.
- FENG, J., HU, H. H. & JOSEPH, D. D. 1994 Direct simulation of the initial value problems for the motion of solid body in a Newtonian fluid. Part 1. sedimentation. *J. Fluid Mech.* **261**, 95–134.
- GLOWINSKI, R., PAN, T. W. & PERIAUX, J. 1994 A fictitious domain method for external incompressible viscous flow modeled by Navier–Stokes equations. *Comput. Methods Appl. Mech. Engng* **112**, 133–148.
- HAPPEL, J. & BRENNER, H. 1986 *Low Reynolds Number Hydrodynamics*. Martinus Nijhoff.
- JOSEPH, D. D. 1990 *Fluid Dynamics of Viscoelastic Liquids*. Springer-Verlag.
- JOSEPH, D. D. 1992 Bernoulli equation and the competition of elastic and inertial pressures in the potential flow of a second order fluid. *J. Non-Newtonian Fluid Mech.* **42**, 385–389.
- JOSEPH, D. D. & LIU, Y. J. 1993 Orientation of long bodies falling in a viscoelastic liquid. *J. Rheol.* **37**(6), 1–22.
- JOSEPH, D. D., LIU, Y. J., POLETTO, M. & FENG, J. 1994 Aggregation and dispersion of spheres falling in viscoelastic liquids. *J. Non-Newtonian Fluid Mech.* **54**, 45–86.
- JOSEPH, D. D., NELSON, J., HU, H. H. & LIU, Y. J. 1992 Competition between inertial pressure and normal stresses in the flow induced anisotropy of solid particles. In *Theoretical and Applied Rheology, Proc. XIth Intl Congr. on Rheology, Brussels, August 17–21* (ed. P. Moldenaers & R. Keunings), pp. 60–65. Elsevier.
- LEAL, L. G. 1975 The slow motion of slender rod-like particles in a second-order fluid. *J. Fluid Mech.* **69**, 305–337.
- LESLIE, F. M. 1961 The slow flow of a visco-elastic liquid past a sphere. *Q. J. Mech. Appl. Maths* **14**, 36–48.
- LIU, Y. J. & JOSEPH, D. D. 1993 Sedimentation of particles in polymer solutions. *J. Fluid Mech.* **255**, 565–595.
- LIU, Y. J., NELSON, J., FENG, J. & JOSEPH, D. D. 1993 Anomalous rolling of spheres down an inclined plane. *J. Non-Newtonian Fluid Mech.* **50**, 305–329.

## CORRIGENDA

A three-dimensional computation of the force and torque on an ellipsoid settling slowly through a viscoelastic fluid

BY J. FENG, D. D. JOSEPH, R. GLOWINSKI AND T. W. PAN

*Journal of Fluid Mechanics*, vol. 283 (1995), pp. 1–16

In transcribing formulae for computation in the above paper, we inadvertently replaced the velocity gradient  $\nabla\mathbf{u}$  with its transpose in the expression for the second-order Rivlin–Ericksen tensor  $\mathbf{A}_2$ . A list of corrections follows.

(i) The direction of the secondary flow  $\mathbf{u}_2$  due to the normal stress perturbation is reversed and  $\mathbf{u}_2$  is in the same sense as  $\mathbf{u}_1$ , the secondary motion caused by inertial perturbation.

(ii) The pressure field  $p_2$  is qualitatively as depicted in figure 10 with high pressure on the left and right sides of the body and low pressure acting on its top and bottom. Pressure  $p_2$  still produces the largest contribution to the torque  $\mathbf{M}_2$ .

(iii) The sense of the torque  $\mathbf{M}_2$  is unchanged, though its magnitude is 2–5 times larger than originally reported. The range of unstable tilt angles (figure 7) is centred around  $60^\circ$ .

The flow induced by the torsional oscillations of an elliptic cylinder

By N. RILEY AND M. F. WYBROW

*Journal of Fluid Mechanics*, vol. 290 (1995), pp. 279–298

There is a transcription error which begins in equation (4.11 *a*).  $\dot{\bar{V}} (= d\bar{V}/d\xi)$  should be replaced by  $\frac{1}{8}\dot{\bar{V}}$  in (4.11 *a*), (4.12), (4.19 *b*) and (4.22 *c*), and in the final paragraph on page 286. None of the results presented is affected by the error.